Local bond-electron-energy relaxation of Mo atomic clusters and solid skins

Zhou, Wei; Bo, Maolin; Wang, Yan; Huang, Yongli; Li, Can; Sun, Chang Qing

2015

Zhou, W., Bo, M., Wang, Y., Huang, Y., Li, C., & Sun, C. Q. (2015). Local bond-electron-energy relaxation of Mo atomic clusters and solid skins. RSC Adv., 5(38), 29663-29668.

https://hdl.handle.net/10356/96191

https://doi.org/10.1039/C5RA00112A

Local bond-electron-energy relaxation of Mo atomic clusters and solid skins

Wei Zhou,[a] Maolin Bo,[a] Yan Wang,[b*] Yongli Huang,[a] Can Li,[c] Chang Q Sun[d*]

[a]*Key Laboratory of Low-Dimensional Materials and Application Technologies , Xiangtan University, Hunan 411105, China*

[b]*School of Information and Electronic Engineering, Hunan University of Science and Technology, Hunan 411201, China*

[c]*Institute of Coordination Bond Metrology and Engineering, School of Materials Science and Engineering, China Jiliang University, Hangzhou 330018, China*

[d]*NOVITAS, School of Electrical and Electronic Engineering, Nanyang Technological University, Singapore 639798, Singapore*

*Email: ywang8@hnust.edu.cn; ecqsun@ntu.edu.sg

Abstract

A combination of the tight-binding theory, bond order-length-strength correlation and nonbonding-electron polarization notion, photoelectron spectrometrics, and density functional theory calculations has enabled us to examine the effect of atomic undercoordination on the local bond-electron-energy relaxation pertaining to Mo(100, 110) skins and atomic clusters. This exercise has led to the following quantitative information: (i) the atomic Mo $3d_{5/2}$ energy level located at 224.862 ± 0.004 eV shifts 2.707 eV deeper upon bulk formation; (ii) skin local bond is subject to 9.80% contraction; (iii) 5.952 e charge transfers from the inner to the outermost skin layer. Furthermore, the E_{4s} level shifts from 61.229 eV for the Mo_{59} to 61.620 eV for the Mo_{15} cluster and the valence band undergoes a 1.057 eV upward shift. The globally positive core-level shift arises from the local quantum entrapment due to bond contraction and strength gain. The densely entrapped core electrons polarize the valence electrons and hence raise the valence band energy.

Keywords: Mo nanoclusters, XPS, DFT, BOLS, core level shift

1. Introduction

Solid skins and atomic clusters have attracted much attention both experimentally and theoretically due to their fascinating chemical and physical properties being different from their bulk counterparts.[1] These abnormal properties include the dilute magnetism[2, 3], catalytic ability[4], creation of Dirac-Fermions for topological insulators[5]. All these properties are closely related to atomic undercoordination induced bond relaxation and electronic structure configuration[1]. Therefore, exploring local electronic properties of systems induced by coordination imperfection would be crucial to improving the understanding of their electronic structure-related properties at the atomic level, such as cohesive energies[6], segregation energies[7], heats of mixing[8], and charge transferring[9].

Molybdenum (Mo) nanoclusters form a kind of interesting material used as media in ultrahigh density magnetic recording[10] and as catalyst in various chemical processes, such as CVD growth of carbon nanotubes[11]. Considerable effort has been made on the X-ray photoelectron spectroscopy (XPS) and density functional theory (DFT) investigation of the undercoordinated Mo systems[12-16]. For example, Lundgren *et al.*[12] found that the 3*d* core-level binding energy of the Mo(110) surface atom is lower by 333±10 meV relative to that of the bulk atoms using XPS. Yakovkin[13, 17] calculated the relaxation of the Mo(111, 112) skins and observed that the surface interlayer contracts by 16.5% and 13.4% in sequence, which is associated with the density redistribution and transformation of the electronic surface states. However, the measured core-level binding energy spectrum represents the mixture of the bulk component and the skin sublayers[18, 19] and the laws governing the energetic behavior of electrons and the electronic properties change of materials for the solid skins and atomic clusters remain unclear. It has been a great challenge to obtain quantitative information regarding the coordination-resolved surface relaxation, binding energy, and the energetic behavior of electrons localized in the solid skins and atomic clusters. Therefore, it is necessary to clarify the contribution of surface local relaxation and reveal the mechanism of the effects of coordination imperfection on the electronic

structure of skins and nanoclusters, which should be useful to understand their electronic structure-related properties at the atomic level.

In this work, we present our examination of the atomic under-coordination effect on the local bond relaxation, binding energy and the associated core-level energy shifts and valence band variation of Mo solid skins and atomic clusters based on bond order-length-strength (BOLS) correlation and nonbonding electron polarization (NEP) premise[20]. Consistency between quantum calculations and photoelectron spectroscopy measurements of Mo skins and nanoclusters confirms our expectations that atomic undercoordination shortens and strengthens the bond, localizes and entraps core electrons, and polarizes the valence charge, which modified the Hamiltonian, atomic cohesive energy, local binding energy density and finally resulted in the unusual properties of Mo skins and nanoclusters.

2. Principles and calculation methods

2.1 BOLS-TB notation

According to the bond order-length-strength (BOLS) correlation[1], the shorter and stronger bonds between under-coordinated atoms result in local densification and quantum entrapment of the core electrons, which makes the valence charges polarise. The bond length and bond strength between under-coordinated atoms are closely associated with the effective atomic coordination number(CN), which is expressed as:

$$\begin{cases} C_i = d_i / d_b = 2 / \left\{1+\exp\left[\left(12-z_i\right)/8z_i\right]\right\} \\ E_i = C_i^{-m} E_b \\ E_C(z) = z_i E_i \end{cases}, \tag{1}$$

where C_i is the coefficient of bond contraction with z_i being the CN of an atom in the ith atomic layer, i counts from the outermost atomic layer inward up to the third layer, d_i and E_i are the bond length and bond energy in the ith atomic layer, respectively, $E_C(z)$ is the atomic cohesive energy. The bond nature indicator m represents how the bond energy changes with bond length. For most metals, m = 1. For nanoclusters, z_1 =

4(1-0.75/K), $z_2 = z_1 + 2$ and $z_3 = 12$, where K represents the dimensional size equaling to R/d_b. R is the real size of the specimen and d_b is the bulk bond length of the corresponding material.

According to the combination of BOLS correlation and the tight-binding theory[21], the single-body Hamiltonian is perturbed by the shorter and stronger bonds, denoted with Δ_H:

$$H(\Delta_H) = -\frac{\hbar^2\nabla^2}{2m} + V_{atom}(r) + V_{crys}(r)(1+\Delta_H), \tag{2}$$

where,

$$\Delta_H = \begin{cases} C_i^{-m} - 1 & (Surface) \\ \tau K^{-1}\sum_{i\le 3} C_i(C_i^{-m} - 1) & (Nanocluster) \end{cases} \tag{3}$$

Note that, the shape factor τ = 1, 2, and 3 corresponds to a thin plate, a cylindrical rod, and a sphere dot, respectively.

Regarding to the core level energies of a material, we mainly focus on two characteristic energies: the vth energy level of an isolated atom $E_v(0)$ and the bulk shift (BS) $\Delta E_v(12) = E_v(12) - E_v(0)$, where z = 12 means the bulk counterpart. The former is the integral of the eigen wave function and the intra-atomic potential, and the latter is its energy shift upon bulk solid formation. Both $E_v(0)$ and $\Delta E_v(12)$ for the particular vth band are intrinsic constant, disregarding the coordination and chemical environment of a given material, which follow the expressions:

$$\begin{cases} E_v(0) = \langle \phi_v(r) | V_{atom}(r) | \phi_v(r) \rangle & (\text{Core level energy}) \\ \Delta E_v(12) = \beta + z\gamma \propto \langle E_b \rangle & (\text{Core level shift}) \\ \beta = \langle \phi_v(r) | V_{crys}(r) | \phi_v(r) \rangle \propto \langle E_b \rangle & (\text{Exchange integral}) \\ \gamma = \langle \phi_v(r) | V_{crys}(r) | \phi_v(r') \rangle \propto \langle E_b \rangle & (\text{Overlap integral}) \end{cases} \tag{4}$$

where, $\phi_v(r)(r \neq r')$ is the Bloch wave function at a specific sites r. z = 0 and 12 represents an isolated atom and an atom in the ideal bulk, respectively. The exchange and overlap integrals are relative to the cohesive energy per bond $<E_b>$. Any perturbation to β and γ causes the shifts of energy level, so the core level energy shifts depend on the bond energy.

With respect to $\Delta E_v(12)$, the under-coordination induced the core level shift $\Delta E_v(z)$ for surface follows[22]:

$$\frac{\Delta E_v(z)}{\Delta E_v(12)} = \frac{E_v(z) - E_v(0)}{E_v(12) - E_v(0)} = \frac{E_z}{E_b} = C_z^{-m} = 1 + \Delta_H$$

$$\text{or} \quad \frac{E_v(z) - E_v(B)}{E_v(z') - E_v(B)} = \frac{C_z^{-m} - 1}{C_{z'}^{-m} - 1} \quad (z' \neq z) \tag{5}$$

With the given surface XPS spectral, we can determine the z-dependent vth energy of an isolated atom $E_v(0)$ and its BS ($\Delta E_v(12)$) by decomposing the spectral into surface components and bulk component with different-coordination number with the relations derived from Eq. (5):

$$\begin{cases} E_v(0) = \dfrac{C_{z'} E_v(z') - C_z E_v(z)}{C_{z'} - C_z} \quad (z' \neq z) \\ \Delta E_v(12) = E_v(12) - E_v(0) \end{cases} \tag{6}$$

Similarly, incorporating the BOLS into the tight-binding theory yields the vth energy level shifts of nanocluster $\Delta E_v(K)$ as follows:

$$\Delta E_v(K) = E_v(K) - E_v(0) = \Delta E_v(12) + \Delta E_v(12)\Delta_H \quad \text{or} \quad E_v(K) = E_v(12) + \Delta E_v(12)\Delta_H \,, \tag{7}$$

where $E_v(K)$ is the XPS peak of the vth energy level of nanocluster. If a cluster is approximately spherical, the relationship of its size and atomic numbers(N) is $K^{-1} = (3N/4\pi)^{-1/3} \approx 1.61N^{-1/3}$,[23] thus, the N-dependence of core-level binding energy $E_v(N)$ can be derived from Eq. (3) and Eq. (7):

$$E_v(N) = E_v(12) + 1.61\tau\Delta E_v(12)\sum_{i\le 3} C_i(C_i^{-m} - 1)N^{-1/3} \tag{8}$$

Generally, the size-induced BE shifts for nanoclusters depends inversely on the size in the form of, $E_v(K)=A+BK^{-1}$, where A and B are constants that can be determined by finding the intercept and the slope of the $E_v(K)$ line, respectively. According to the relationship of K and N, we can deduce the form of N versus BE shift into $E_v(N) = A+1.61BN^{-1/3} = A+B' N^{-1/3}$. Comparing the experimental scaling relationship with the theoretical expression yields,

$$E_v(N) = \begin{cases} E_v(12) + 1.61\tau\Delta E_v(12)\sum_{i\le 3} C_i(C_i^{-m} - 1)N^{-1/3} & \text{(BOLS theory)} \\ A + B'N^{-1/3} & \text{(Measurement)} \end{cases} \tag{9}$$

Equating the BOLS theory prediction to measurements gives the relation:

$$\begin{cases} A = E_v(12) \\ B' = 1.61\tau\Delta E_v(12)\sum_{i\le 3} C_{z_i}(C_{z_i}^{-m} - 1) \end{cases} \tag{10}$$

This also allows us to determine the vth energy level of an isolated atom and its bulk shift possible:

$$\begin{cases} E_v(0) = A - B' \Big/ \left(1.61\tau \sum_{i\le 3} C_{z_i}(C_{z_i}^{-m} - 1)\right) & \text{isolated atomic energy level} \\ \Delta E_v(12) = B' \Big/ \left(1.61\tau \sum_{i\le 3} C_{z_i}(C_{z_i}^{-m} - 1)\right) & \text{BS} \end{cases} \tag{11}$$

Using Eq. (6) or (11), we can readily determine the energy level $E_v(0)$ of an isolated atom and its BS $\Delta E_v(12)$ by analyzing the measurements. Note that, for the same element, the $E_v(0)$ and $E_v(12)$ are intrinsic constants for all surfaces, disregarding the coordination and chemical environment of a given material.

For the detectable quantities can be directly connected to the bond identities such as bond nature, order, length and strength, we are able to predict coordination number resolved the local bond strain ($\varepsilon(z)$), relative binding energy density(δE_D), relative core-level binding energy shift (δE_z), and the relative cohesive energy per atom (δE_C) in the surface skins,

$$\begin{cases} \varepsilon(z) = C_z - 1(\%) \\ \delta E_D = E_D(z)/E_D(12) - 1 = C_z^{-4} - 1\ (\%) \\ \delta E_z = \Delta E_v(z)/\Delta E_v(12) - 1 = C_z^{-m} - 1\ (\%) \\ \delta E_C = E_C(z)/E_C(12) - 1 = z_{ib} C_z^{-m} - 1\ (\%) \end{cases} \tag{12}$$

with $z_{ib} = z_i/12$. Subscript i denote the atomic layers counted from the outermost inwards. These basic quantities determine the related properties at the specific atomic site. For instance, atomic cohesive energy dominates the critical temperature of melting[24-26] and the binding energy density determines the elastic modulus[27, 28].

2.2 DFT calculations

In order to verify the BOLS predictions on the coordination imperfection induced the core-level entrapment and the valence charge polarization, we conducted DFT calculations on the optimal bond relaxation, charge transfer[29], and the energetic distribution of the core band and valence states of Mo nanoclusters with different

structures[30, 31], as shown in Fig. 1. Moreover, we also compared the computational results with the photoelectron spectroscopy measurements.

The DFT calculations were performed using the DMol3 code with a double numeric plus polarization basis set[32]. During the DFT calculations, the potentials of core electrons were assumed to be DFT semi-core pseudopotential[33]. The DFT exchange-correlation potential utilized the local-density approximation (LDA), with the PWC function for geometry and electronic structures[23, 34]. PWC is the default functional for DMol3 calculations. The self-consistency threshold of total energy was set at 10^{-6} au in calculations. The tolerance limit for the energy, forces, and displacement in geometry optimization were taken at 10^{-5} Hartree, 0.002 Hartree/Å, and 0.005 Å, respectively.

3. Results and Discussion

3.1 Surface core level quantum entrapment

To better understand the effects of coordination imperfection and the physical origin of surface core level shift, we decomposed the Mo $3d_{5/2}$ spectra of the clean surface Mo(100) and Mo(110) in Fig. 2[12, 35]. Obeying the constraints given in Eq.(5), the spectra from clean surface of Mo(100) and Mo(110) specimen were decomposed with three components, corresponding to the bulk (B), surface skins S_2 and S_1 from higher (smaller absolute value) to lower BE after the subtraction of the Tougaard background[36]. Table 1 summarizes the optimal component energies, the corresponding z_i, and the z-resolved local bond strain (ε_z), the relative binding energy density (δE_D), the relative core-level binding energy shift (δE_z), and the relative cohesive energy per atom (δE_C)were summarized.

From the decomposition, we obtained the $E_{3d_{5/2}}(0)$, $\Delta E_{3d_{5/2}}(z_i)$ and the standard deviation (σ) by using a least root-mean-square method. A fine-tuning of the CN values of the components will minimize σ and improve the accuracy of the effective CN for each sublayer. It has been derived that the $3d_{5/2}$ BE of bulk and surface skin shift deeper from 2.707 to 3.100 eV with respect to that of the isolated Mo (224.862 ±

0.004 eV) atoms. The following describes the obtained the *z*-resolved $3d_{5/2}$ BE shift for Mo skins:

$$E_{3d_{5/2}}\left(C_{z_i}\right)=\left\langle E_{3d_{5/2}}\left(0\right)\right\rangle \pm \sigma + \Delta E_{3d_{5/2}}\left(B\right)C_{z_i}^{-m}=224.862\pm 0.004+2.707C_{z_i}^{-1}$$

These refinement led to the effective atomic CNs of the top (second) Mo (100, 110) atomic layers as 3.98 (5.16) and 3.95 (5.83). With the derived *z* value and the $3d_{5/2}$ BE for each XPS component, we could predict the *z*-resolved local bond strain $\varepsilon_z(z)$, the relative BE shift $\delta E_z(z)$, the relative atomic cohesive energy $\delta E_C(z)$ and the relative binding energy density $\delta E_D(z)$ of the Mo surface skins, as shown in Fig. 3. It is found that the undercoordination-induced local bond strain contracted, relative binding energy density enhanced, relative atomic cohesive energy weakened and relative core-level binding energy shifted positively up to 12.67%, 71.92%, 62.31%, 14.51%, respectively, for the outermost three atomic layer of Mo surface. The fundamental information we have derived is of great importance in determining the surface properties and surface processes.

3.2 Bond contraction, core level entrapment and valence charge polarization

According to the BOLS-NEP, bonds between under-coordinated atoms in low-dimensional system are shorter and stronger, which makes the potential well deeper and hence the core-level energy levels of these atoms drop correspondingly. Polarization induced by the densely trapped bonding electrons will take place if nonbonding electrons exist. To further confirm our predictions, we performed the bond contraction, binding energy and valence local DOS of Mo_N clusters described by Finnis–Sinclair potentials[30] with different size and structure from the perspective of DFT calculations, as shown in Fig.1. From the DFT results of the bond length and bond contraction between atoms of Mo_N clusters, we can find that atoms in the cluster interior have no contraction equaling to the ideal distance of the corresponding bulk atom, while the skin atoms with under-coordinated number contract, which was listed in Table 2. And the smaller the CN is, the stronger the bond contracts, that is, the extent of these clusters skin atoms contraction depends on its CN. The results agree well with the reported bond contraction of Ag, Au, Cu, Ni, Pd, Pt, Fe atomic chains[37,

[38].We also estimated the charge flow of these Mo nanoclusters using the Mulliken population analysis[29] and found that the electrons flowed from the inner to the outermost layer of the clusters, which were also listed in Table 2. The negative sign represents charge loss. It indicated that the interaction between under-coordinated atoms induced quantum entrapment, and hence resulted in the core electron entrapment from the local sites and the densification of charge and energy.

Fig. 4 showed the 4*s* BE (a) and LDOS (b) for the $C_{2v}15$, $C_2 28$, $D_s 20$, $C_2 28$, $C_s 47$, $C_2 51$ and $O_h 59$ structures calculated by DFT. It is readily shown that the 4*s* level shifts from 61.229 eV for the Mo_{59} nanocluster to 61.620 eV for the Mo_{15} nanocluster while the LDOS peak shifts from -0.897 eV for Mo_{59} to 0.160 eV for Mo_{15}. This illustrates that both the core-level atoms localization-entrapment and the valence charge polarization take place in these Mo nanoclusters, and hence lead to positive core level shift and negative valence band shift. Both of them exhibit stronger bonds with the size decreasing. These DFT calculations further confirmed our BOLS-NEP predictions.

3.3 *N*-resolved $E_v(N)$

Choosing Mo_{59} cluster for the standard reference, we can obtain its dimensional size $K = R/d_b = 1.714$, for R is 4.672 Å and the d_b is 2.725 Å of Mo_{59}. According to Eq. (1), we can estimate $z_1 = 4(1\text{-}0.75/K) = 2.25$ and $z_2 = z_1+2 = 4.25$ and thus obtain C_1 and C_2 being 0.7356 and 0.8865, respectively. Fig.5 shows that $E_{4s}(N)$ of Mo nanoclusters depends linearly on $N^{-1/3}$, which gives the *y*-intercept and the slope are 60.760 and 2.062, respectively. According to the *y*-intercept and slope derived from *N*-induced Mo $E_{4s}(N)$ and Eq. (11), we can obtain:

$$E_{4s}(12) = 60.760\text{eV and } \Delta E_{4s}(12) = 3.389/\tau$$

Because the shape of Mo nanocluster is not an ideal sphere, the shape factor τ is uncertain, which should be greater than unity and smaller than three. Although the bulk shift of Mo $\Delta E_{4s}(12)$ is absent, we have obtained the $\Delta E_{3d5/2}(12) = 2.707$ eV. Though the shifts of different core level energy have a slight deviation, but the core level band of nanoclusters shifts down as a whole, so we assume the BS shift of E_{4s}

and $E_{3d5/2}$ the same to obtain the information of E_{4s}. Therefore, we can determine the value of τ being 1.252. Thus, N-resolved $E_{4s}(N)$ follows:

$$E_{4s}(N) = E_{4s}(12)+1.61\tau\Delta E_{4s}(12)\sum_{i\leq 3} C_i(C_i^{-m}-1)N^{-1/3} = 60.760 + 2.062N^{-1/3}$$

Such a consistency of DFT calculations and BOLS predictions evidences that the local bond contraction and quantum entrapment will lead to a densification of mass, charge and energy near the undercoordianted atomic site, which resulted in the enhancement of the Hamiltonian and hence the positive BE shifts for Mo skins and nanoclusters. Therefore, the interaction between undercoordianted atoms dominates the behavior of BE shifts.

4. Conclusion

Consistency between DFT calculations and photoelectron spectroscopy measurements confirmed our BOLS-NEP predictions of the atomic CN effects on the local bond relaxation, electron binding-energy shift, and valence charge transfer of Mo skins and nanoclusters. It was clarified that Mo $3d_{5/2}$ ($4s$) shifts positively by 2.707 eV from a value of 224.862 (58.053) eV for an isolated atom to 227.569 (60.760) eV for the bulk. The interaction between under-coordinated atoms caused local strain, local densification and entrapment of the core electrons, as well as valence charge polarization, which perturbed the Hamiltonian and hence dominated the unusual behaviour of Mo surfaces and nanoclusters. Findings will be useful to apply Mo skins and nanoclusters in practical application, such as catalytic enhancement, applications in electronics and optics.

Acknowledgment

We gratefully acknowledge financial support from the NSF (Grants No. 11172254 and No.11402086).

References

1. C. Q. Sun, *Relaxation of the Chemical Bond*. (Springer, Heidelberg, 2014).
2. P. Sahoo, H. Djieutedjeu and P. F. P. Poudeu, Journal of Materials Chemistry A **1** (47), 15022–15030 (2013).
3. G. L. Nealon, B. Donnio, R. Greget, J. P. Kappler, E. Terazzi and J. L. Gallani, Nanoscale **4** (17), 5244-5258 (2012).
4. R. Q. Zhang, Y. Lifshitz, D. D. Ma, Y. L. Zhao, T. Frauenheim, S. T. Lee and S. Y. Tong, The Journal of Chemical Physics **123** (14), 144703-144703 (2005).
5. J. R. B. Gomes, F. Illas and B. Silvi, Chemical Physics Letters **388** (1–3), 132-138 (2004).
6. W. H. Qi, M. P. Wang and G. Y. Xu, Chemical Physics Letters **372** (5-6), 632-634 (2003).
7. A. Rosengren and B. Johansson, Physical Review B **23** (8), 3852-3858 (1981).
8. A. Belonoshko, N. Skorodumova, A. Rosengren and B. Johansson, Physical Review B **73** (1), 012201- 012201 (2006).
9. J. A. Oliveira, W. B. De Almeida and H. A. Duarte, Chemical Physics Letters **372** (5-6), 650-658 (2003).
10. P. Entel, M. E. Gruner, G. Rollmann, A. Hucht, S. Sahoo, A. T. Zayak, H. Herper and A. Dannenberg, Philosophical Magazine **88** (18-20), 2725-2738 (2008).
11. K. Goss, A. Kamra, C. Spudat, C. Meyer, P. Kögerler and C. Schneider, physica status solidi (b) **246** (11‐12), 2494-2497 (2009).
12. E. Lundgren, U. Johansson, R. Nyholm and J. N. Andersen, Phys. Rev. B **48** (8), 5525-5529 (1993).
13. I. N. Yakovkin, M. Kuchowicz, R. Szukiewicz and J. Kołaczkiewicz, Surface Science **600** L240-L244 (2006).
14. J. Andersen, D. Hennig, E. Lundgren, M. Methfessel, R. Nyholm and M. Scheffler, Physical Review B **50** (23), 17525 (1994).
15. S. Ismail-Beigi and T. Arias, Physical Review Letters **84** (7), 1499 (2000).
16. R. Trivedi, K. Dhaka and D. Bandyopadhyay, RSC Advances **4** (110), 64825-64834 (2014).
17. I. Yakovkin, The European Physical Journal B-Condensed Matter and Complex Systems **44** (4), 551-555 (2005).
18. M. Patanen, C. Nicolas, X. J. Liu, O. Travnikova and C. Miron, Physical Chemistry Chemical Physics **15** (25), 10112-10117 (2013).
19. D. M. Riffe and G. K. Wertheim, Physical Review B **47** (11), 6672-6679 (1993).
20. C. Q. Sun, Nanoscale **2** (10), 1930-1961 (2010).
21. M. A. Omar, *Elementary solid state physics: principles and applications*. (Addison-Wesley Reading, MA, USA:, 1975).
22. C. Q. Sun, Physical Review B **69** (4), 045105-045112 (2004).
23. M. Bo, Y. Wang, Y. Huang, W. Zhou, C. Li and C. Q. Sun, Journal of Materials Chemistry C **2** (30), 6090-6096 (2014).
24. C. Q. Sun, Y. Shi, C. M. Li, S. Li and T. C. A. Yeung, Phys. Rev. B **73** (7), 075408 (2006).
25. C. Cazorla, D. Alfè and M. J. Gillan, J Chem Phys **130** (17), 174707 (2009).
26. C. Q. Sun, Y. Wang, B. K. Tay, S. Li, H. Huang and Y. B. Zhang, The Journal of Physical Chemistry B **106** (41), 10701-10705 (2002).

27. X. J. Liu, J. W. Li, Z. F. Zhou, L. W. Yang, Z. S. Ma, G. F. Xie, Y. Pan and C. Q. Sun, Appl. Phys. Lett. **94**, 131902 (2009).
28. C. Cazorla, D. Alfè and M. J. Gillan, Computational Materials Science **50** (9), 2732-2735 (2011).
29. M. Segall, C. Pickard, R. Shah and M. Payne, Molecular Physics **89** (2), 571-577 (1996).
30. J. Elliott, Y. Shibuta and D. Wales, Philosophical Magazine **89** (34-36), 3311-3332 (2009).
31. J. Elliott and Y. Shibuta, Journal of Computational and Theoretical Nanoscience **6** (7), 1443-1451 (2009).
32. B. Delley, Journal of Chemical Physics **92** (1), 508-517 (1990).
33. B. Delley, Physical Review B **66** (15), 155125-155133 (2002).
34. J. P. Perdew and Y. Wang, Physical Review B **45** (23), 13244-13249 (1992).
35. E. Minni and F. Werfel, Surface and Interface Analysis **12** (7), 385-390 (1988).
36. Y. Wang, Y. G. Nie, J. S. Pan, L. K. Pan, Z. Sun, L. L. Wang and C. Q. Sun, Physical Chemistry Chemical Physics **12** (9), 2177-2182 (2010).
37. A. Kara and T. S. Rahman, Physical Review Letters **81** (7), 1453-1456 (1998).
38. F. Baletto, R. Ferrando, A. Fortunelli, F. Montalenti and C. Mottet, The Journal of Chemical Physics **116** (9), 3856-3863 (2002).

Table and Figure captions:

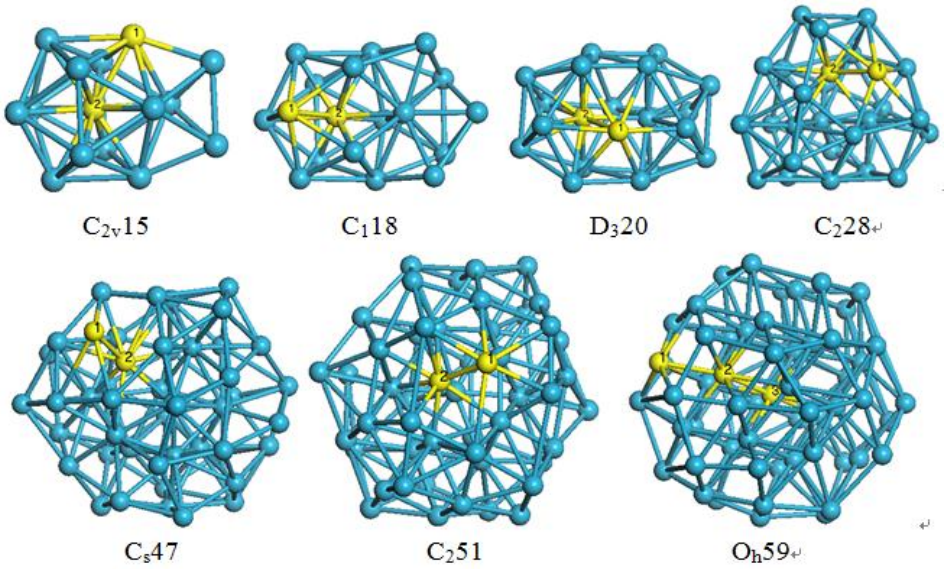

Figure 1 Global minima of Mo_N clusters described by Finnis–Sinclair potentials[30].

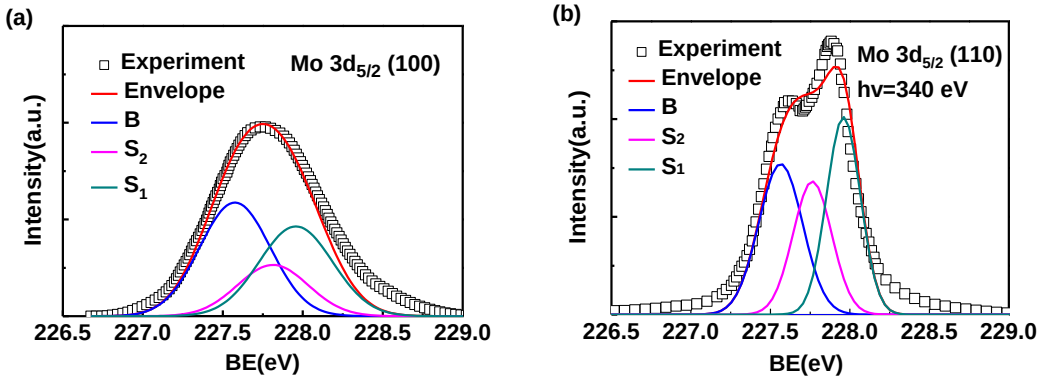

Figure 2 Decomposition of the Mo $3d_{5/2}$ spectra for (a) Mo(100)[35] and (b) Mo(110)[12] surfaces with three Gaussian components representing the bulk B, S_2, and S_1 components from higher(smaller absolute value) to lower BE, which obey the BOLS constraints given in Eq. (5). The related derived information is listed in Table 1.

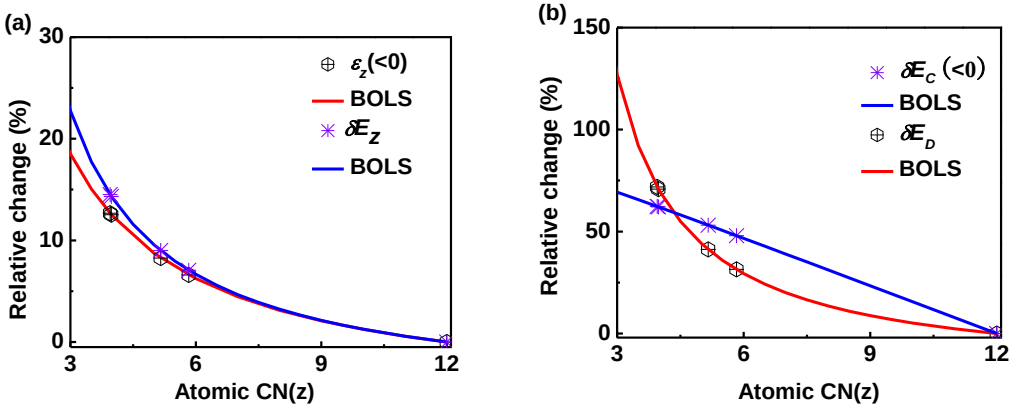

Figure 3 CN-resolved (a) local bond contraction $\varepsilon_z(z)$,relative BE shift $\delta E_z(z)$, (b) relative atomic cohesive energy $\delta E_C(z)$ and relative binding energy density $\delta E_D(z)$.

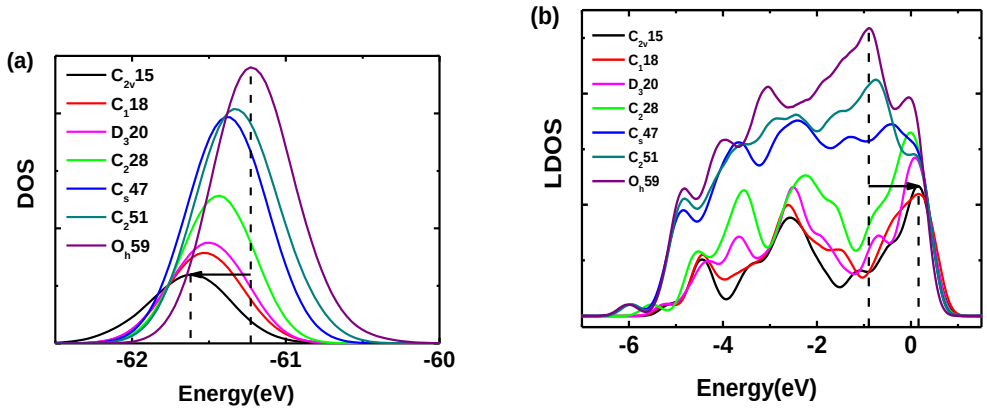

Figure 4 Undercoordination induced (a) core-level energy level entrapment and (b) valence band polarization of Mo clusters($C_{2v}15$, $C_1$18, D_s20, $C_2$28, C_s47, $C_2$51, O_h59), indicating the extent of entrapment and polarization depends on the cluster size.

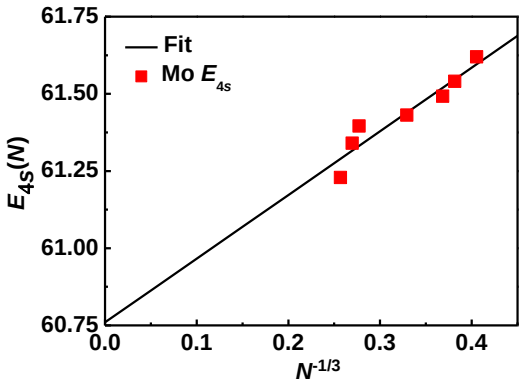

Figure 5 The N-resolved E_{4s} of free Mo_N nanoclusters.

Table 1 Atomic-layer and crystal-orientation resolved the effective CN(z), bond contraction (ε_z), relative BE shift (δE_z), relative atomic cohesive energy (δE_C), and the relative binding energy density (δE_D)determined from the measured XPS profiles of Mo (100) and (110) surfaces under the established approach and the criteria.

	i	$E_{3d^{5/2}}(i)$	z	$-\varepsilon_z$	δE_z (%)	$-\delta E_C$(%)	δE_D(%)
Bulk	B	227.570	12.00	0	0	0	0
Mo(100)	S_2	227.813	5.16	8.27	9.01	53.13	41.21
	S_1	227.957	3.98	12.53	14.32	62.08	70.81
Mo(110)	S_2	227.761	5.83	6.60	7.07	47.98	31.43
	S_1	227.962	3.95	12.67	14.51	62.31	71.92

Table 2 DFT calculation results of the bond length (d_i), bond contraction coefficient (C_z) and charge transfer of Mo_N clusters. The charge transfer (Mulliken population analysis) of different structures reveals charge flow from the inner to the outermost atomic shells due to the quantum entrapment.

Structure	d_{12}(Å) (Atomposition 1-2)	C_z–1(%)	Charge Transfer (e) (Shell layer1-2)

$C_{2v}15$	2.612	-4.147	-1.028
$C_1 18$	2.597	-4.697	-1.283
$D_3 20$	2.574	-5.541	-1.333
$C_2 28$	2.581	-5.284	-2.035
$C_s 47$	2.493	-8.514	-4.137
$C_2 51$	2.458	-9.798	-4.571
$O_h 59$	2.560	-6.055	-5.952